Assessment of the size, position, and optical properties of breast tumors *in vivo* by noninvasive optical methods

Sergio Fantini, Scott A. Walker, Maria Angela Franceschini, Michael Kaschke, Peter M. Schlag, and K. Thomas Moesta

We present a method for the noninvasive determination of the size, position, and optical properties (absorption and reduced scattering coefficients) of tumors in the human breast. The tumor is first detected by frequency-domain optical mammography. It is then sized, located, and optically characterized by use of diffusion theory as a model for the propagation of near-infrared light in breast tissue. Our method assumes that the tumor is a spherical inhomogeneity embedded in an otherwise homogeneous tissue. We report the results obtained on a 55-year-old patient with a papillary cancer in the right breast. We found that the tumor absorbs and scatters near-infrared light more strongly than the surrounding healthy tissue. Our method has yielded a tumor diameter of 2.1 ± 0.2 cm, which is comparable with the actual size of 1.6 cm, determined after surgery. From the tumor absorption coefficients at two wavelengths (690 and 825 nm), we calculated the total hemoglobin concentration (40 ± 10 μM) and saturation (71 ± 9%) of the tumor. These results can provide the clinical examiner with more detailed information about breast lesions detected by frequency-domain optical mammography, thereby enhancing its potential for specificity.

OCIS codes: 170.3830, 300.0300, 300.1030, 290.0290.

1. Introduction

Optical mammography is a noninvasive imaging modality that employs visible and near-infrared light (typically in the wavelength range 670–970 nm) to detect breast cancer. It was first proposed in 1929,[1] and it evolved in the so-called diaphanography[2] and light scanning[3] in the 1970s and early 1980s. The basic approach consisted of illuminating one side of the female breast with a continuous-wave (cw) light beam, while the examiner looked for regions of lower transmitted intensity (shadows) on the opposite side. The method evolved empirically and was eventually abandoned in the early 1990s when a multicenter study demonstrated its inferior performance with respect to x-ray mammography.[4] A more systematic approach in cw light mammography has been recently proposed by Yamashita and Kaneko, who employed a narrow light beam and a collimated detector.[5] Recent progress in the understanding of light propagation in breast tissue and the development of time-resolved techniques (in either the time- or frequency-domain) in tissue spectroscopy have yielded new approaches in optical mammography. We recently reported initial clinical results obtained with a new frequency-domain light mammography apparatus[6] that operates at two wavelengths in the near infrared. In this frequency-domain approach, the optical mammograms show an improved image contrast with respect to diaphanography, and the images are displayed in real time on a computer screen during the exam without requiring any additional manipulation. Ongoing clinical trials are giving promising results.[7,8] However, our previous algorithm of data analysis[9] is aimed only at tumor detection, and it does not fully exploit the potential of frequency-domain optical mammography because it does not afford the discrimination of absorbing and scattering inhomogeneities. In this paper we present an additional analysis of the optical mammograms that complements our previous approach and allows us to quantify the size, the position, and the optical properties of breast tumors *in vivo*. The op-

S. Fantini, S. A. Walker, and M. A. Franceschini are with the Laboratory for Fluorescence Dynamics, Department of Physics, University of Illinois at Urbana-Champaign, 1110 West Green Street, Urbana, Illinois 61801-3080. K. T. Moesta and P. M. Schlag are with the Department of Surgery and Surgical Oncology, Robert Roessle Hospital and Tumor Institute at the Max-Delbruck Center for Molecular Medicine, Humboldt University, D 13122 Berlin, Germany. M. Kaschke is with Carl Zeiss, Medical-Optical Instruments, D 73446 Oberkochem, Germany.

Received 4 August 1997; revised manuscript received 8 December 1997.

0003-6935/98/101982-08$15.00/0

tical properties of the tumor are described by its absorption (μ_a) and reduced scattering (μ_s') coefficients, both in units of inverse centimeters. From the absorption coefficients at two wavelengths (690 and 825 nm), we calculate the hemoglobin concentration and saturation in the area of the lesion. This analysis provides a new approach that may result in a higher specificity of optical mammography.

2. Theory

Our theoretical approach to describe light propagation in breast tissue is based on diffusion theory. The tumor is modeled by a spherical inhomogeneity of diameter d embedded in an otherwise homogeneous tissue. We indicate the absorption and the reduced scattering coefficients of the background healthy tissue with μ_{a0} and μ_{s0}', respectively. The optical coefficients of the tumor are indicated by $\mu_a^{(t)}$ and $\mu_s'^{(t)}$. In this way, we section the breast tissue in two regions: one is the uniform background and the other is the spherical tumor. The analytical solution for the problem of a spherical photon density wave of angular frequency ω scattered by a spherical inhomogeneity embedded in a uniform, infinite, turbid medium has been given by Boas *et al.*[10] The solution for the scattered photon density (U_{scatt}) out of the sphere is given by an infinite series whose terms contain the spherical harmonics $Y_{l,m}(\theta, \varphi)$ and the spherical Bessel $[j_l(x)]$ and Neumann $[n_l(x)]$ functions[10]:

$$U_{\text{scatt}} = \sum_{l,m} A_{l,m}[j_l(k_0 r) + i n_l(k_0 r)]Y_{l,m}(\theta, \varphi), \quad (1)$$

where $k_0 = [(-\nu\mu_{a0} + i\omega)/\nu D_0]^{1/2}$, ν is the speed of light in the medium, $D_0 = 1/(3\mu_{a0} + 3\mu_{s0}')$, and the coefficients $A_{l,m}$, determined by the boundary conditions, are given in Ref. 10. It is possible to generalize this solution to the slab geometry (which best describes the sampling configuration used in our light mammography apparatus) by use of the method of images[11] (where one must introduce images for both the photon source and the sphere) and by application of extrapolated boundary conditions.[12] This approach to the solution of the sphere-in-slab problem is implemented in the Photon Migration Imaging software[13] that we used to perform the fits to our experimental data.

3. Instrument for Frequency-Domain Optical Mammography

The frequency-domain light mammography apparatus (LIMA) is described in detail in Ref. 6. This instrument operates in transmission mode, with the breast slightly compressed between two glass plates. The light sources are two laser diodes emitting at 690 and 825 nm, respectively. The average optical power on the breast is approximately 10 mW. The two laser beams are collimated and made collinear to illuminate a 3-mm^2 spot on the breast. On the opposite side of the breast, the transmitted light is collected by an optical fiber (5 mm in diameter) that sends the optical signal to a photomultiplier tube (PMT) detector. The intensities of the laser diodes are modulated at a frequency of 110 MHz. We obtained the amplitude ac and the phase Φ of the photon density wave launched into the breast tissue by heterodyning and digital acquisition methods.[14] A schematic diagram of the instrument and a vertical section of the compressed breast are shown in Fig. 1. The distance between the light source and the detector fiber is determined by the separation between the glass plates (L). This separation is $L = 4$ cm for the case reported in this paper. The light source and the detector fiber are scanned in tandem and are always kept collinear, facing each other. This optical mammography unit acquires a full image of the breast in approximately 3 min.

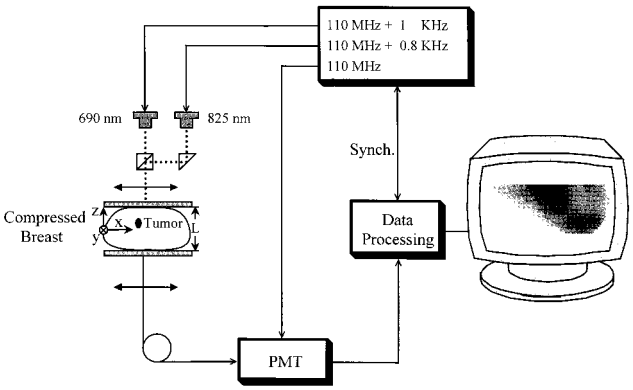

Fig. 1. Schematic diagram of the frequency-domain LIMA. The two light sources are laser diodes emitting at 690 and 825 nm. Their intensities are modulated at a frequency of 110.001 MHz and 110.0008 MHz, respectively, by a radio-frequency (rf) oscillator. The two laser beams are collimated and made collinear, and they illuminate one side of the compressed breast. L is the separation between the plates for breast compression. On the opposite side of the breast, an optical fiber collects the optical signal and sends it to the PMT detector. The PMT gain is modulated at a frequency of 110 MHz to provide a beating with the frequencies of the detected signals at the two wavelengths. The data processing, which is synchronized (Synch.) with the rf oscillator, consists of recovering the amplitude and phase information at the two wavelengths and of applying the algorithm for edge effect corrections. The frequency-domain optical mammogram is displayed on the screen in real time during the exam.

4. Methods and Results

Figures 2(a) and 2(b) show the optical mammograms at 690 and 825 nm, respectively, taken in the mediolateral projection on the right breast of a 55-year-old patient affected by breast cancer. A histological exam following optical mammography has shown that this tumor is a papillary cancer, whose size has been determined, after surgery, to be 1.6 cm. The points in Fig. 3(a) and Fig. 4(a) represent the frequency-domain data for ac, and the points in Fig. 3(b) and Fig. 4(b) represent the frequency-domain data for the phase. The data points are collected at 690 nm in Figs. 3(a) and 3(b) and at 825 nm in Figs. 4(a) and 4(b) along a particular line that includes the tumor position [the tumor is approximately centered

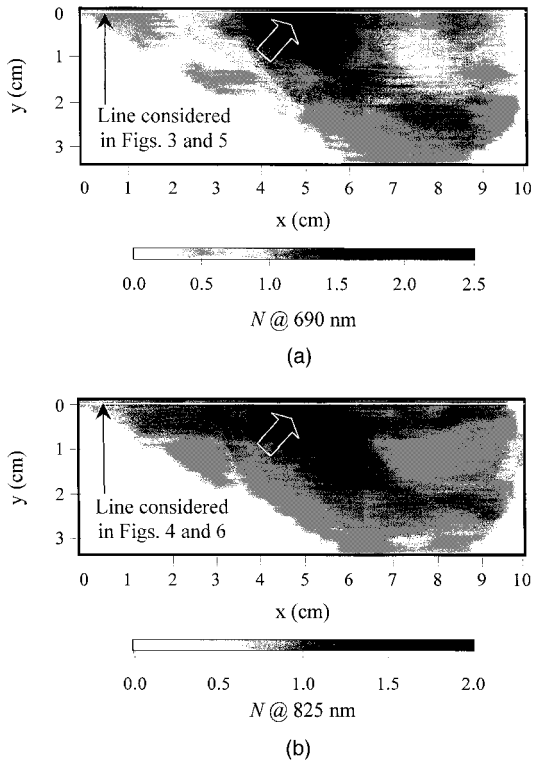

Fig. 2. Frequency-domain optical mammograms [(a), 690 nm; (b), 825 nm] of the right breast (mediolateral projection) of a 55-year-old patient affected by breast cancer. The tumor location is indicated by the white arrow. The scanned line at $y = 0$, indicated in the figures, is considered for the application of our method aimed at the optical characterization of the tumor.

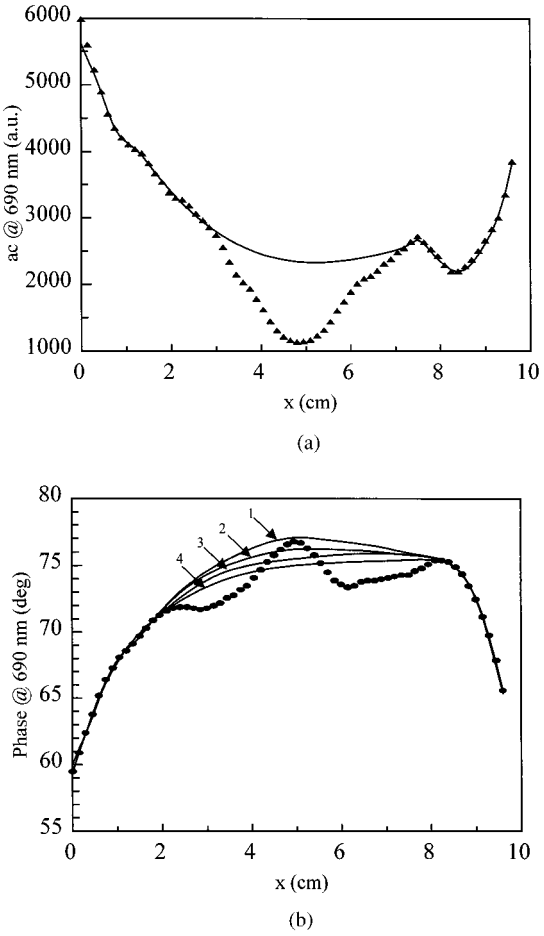

Fig. 3. (a) Filled triangles represent the experimental ac amplitude and (b) solid circles represent the phase at 690 nm measured along the scanned line indicated in Fig. 2(a). The tumor is centered at $x^{(t)} = 4.9$ cm. The continuous curves are the fits of a smooth function to the experimental data out of the tumor region. We considered four different phase curves (labeled 1–4 in (b)] to estimate the sensitivity of our method to a particular choice for the background phase.

at $x^{(t)} = 4.9$ cm, $y^{(t)} = 0$]. This particular line ($y = 0$) is indicated in the optical mammograms (Figs. 2(a) and 2(b)). The edge effects, which are due mainly to the decrease in the breast thickness as the scanner approaches the edge of the breast, cause a strong increase in the ac amplitude and a strong decrease in the phase in the initial and final part of the scanned line (see Figs. 3 and 4). In our previous research we reduced the edge effects by using the phase information to determine the breast thickness at each image pixel.[9] The suppression of the edge effects resulted in an improved image contrast.[8] Our edge-effect-corrected optical mammograms report a dimensionless parameter, that we call N, on a linear gray scale (see Fig. 2). These mammograms can detect breast tumors but they do not give information about their size, depth, and optical properties. In this paper we proceed one step further by exploiting the phase information, in addition to the intensity information, to determine the size, depth, and optical properties of the tumor. Our approach is based on the three steps outlined below.

(1) We first detect and roughly localize the tumor in the edge-effect-corrected optical mammogram (Fig. 2). In that image, we consider the scanned line that includes the tumor ($y = 0$ in the case reported here). Given the approximate location of the tumor along this line [around $x^{(t)} = 4.9$ cm], we proceed by fitting the data out of the tumor region with a smooth curve. In the case shown here, the raw data indicate that the tumor affects the phase at $|x - x^{(t)}| \leq 3$ cm, and the ac amplitude at $|x - x^{(t)}| \leq 2$ cm. The smooth curve fitted to the data points out of the tumor, i.e., the ones not affected by the tumor, represents the data that one would ideally collect in the absence of the tumor, but in the presence of edge effects. For this reason we call it the background curve. The background curve for the ac amplitude [$\mathrm{ac}_{\mathrm{bgr}}(x)$] is shown by the continuous curve in Fig. 3(a) (690 nm) and in Fig. 4(a) (825 nm). In Figs. 3(b) (690 nm) and 4(b) (825 nm) we show four possible background curves for the phase data [$\Phi_{\mathrm{bgr}}(x)$]. We obtained the background curves by superimposing a third-degree polynomial and four to six Gaussian peaks. Although there is little ambiguity in the determination of $\mathrm{ac}_{\mathrm{bgr}}(x)$, several curves appear to be reasonable choices for $\Phi_{\mathrm{bgr}}(x)$.

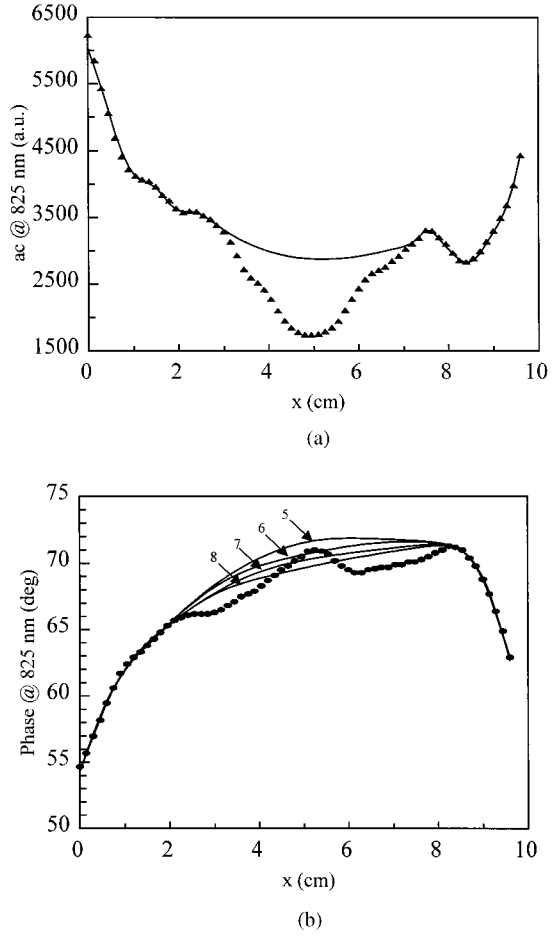

Fig. 4. (a) Filled triangles represent the experimental ac amplitude and (b) filled circles represent the phase at 825 nm measured along the scanned line indicated in Fig. 2(b). The tumor is centered at $x^{(t)} = 4.9$ cm. The continuous curves are the fits of a smooth function to the experimental data out of the tumor region. We considered four different phase curves [labeled 5–8 in (b)] to estimate the sensitivity of our method to a particular choice for the background phase.

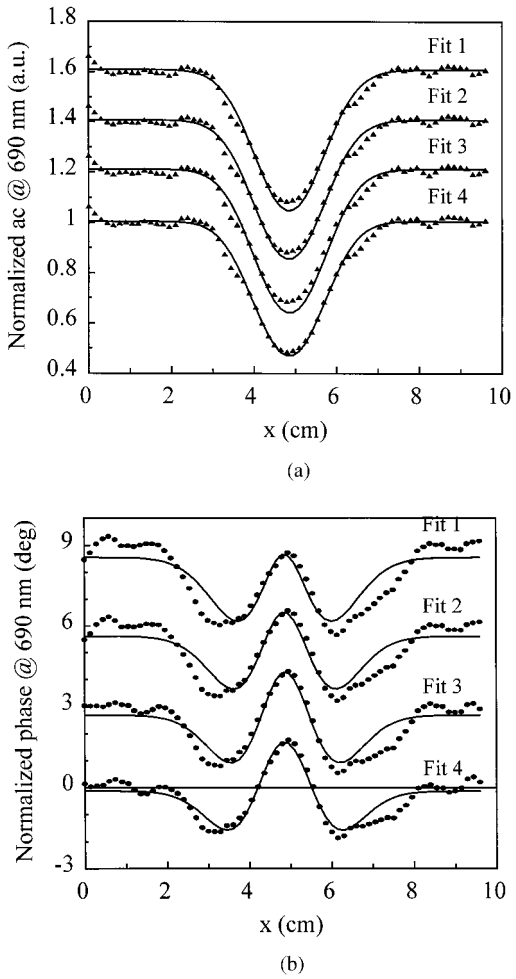

Fig. 5. Normalized data at 690 nm and fits with the analytical solution for the sphere-in-slab problem (curves). (a) ac, solid triangles; (b) phase, solid circles. The four fits [numbered 1–4 in (a) and (b)] correspond to the four different background phase curves shown in Fig. 3(b). In (a), the ac data and fits numbered 1, 2, and 3 were shifted by 0.6, 0.4, and 0.2 a.u., respectively, for clarity. In (b), the phase data and fits numbered 1, 2, and 3 were shifted by 9, 6, and 3 deg, respectively, for clarity.

To evaluate the sensitivity of our method to the choice of $\Phi_{bgr}(x)$, we considered all four different curves $\Phi_{bgr}(x)$ that are shown in Figs. 3(b) and 4(b). We observe that superficial inhomogeneities (such as superficial blood vessels) have a strong effect on the ac, and a negligible effect on the phase {for example, the evident negative bump at $x \sim 8.3$ cm in the ac traces [Figs. 3(a) and 4(a)] does not have a visible corresponding feature in the phase traces [Figs. 3(b) and 4(b)]}. For this reason, we treated the ac and phase background curves independently.

(2) As a second step, we divide the measured ac $[ac(x)]$ by the background ac $[ac_{bgr}(x)]$, and we subtract the background phase $[\Phi_{bgr}(x)]$ from the measured phase $[\Phi(x)]$. The resulting normalized ac $[ac_{norm}(x) = ac(x)/ac_{bgr}(x)]$ and phase $[\Phi_{norm}(x) = \Phi(x) - \Phi_{bgr}(x)]$ show the effect of the tumor but not that of the edge effects. The normalized ac and phase are shown in Figs. 5(a) and 5(b) (690 nm) and in Figs. 6(a) and 6(b) (825 nm).

(3) On the normalized data, we perform the fit with the analytical solution to the diffusion problem of light transmission through an infinite slab-shaped turbid medium that contains a spherical inhomogeneity. The resulting fits are shown by the continuous curves in Figs. 5 and 6, where the numbered fits correspond to the different phase background curves in Figs. 3(b) and 4(b). We performed the fit by simultaneously fitting the ac and phase data, by minimization of the global χ^2. We took the ac error to be 3% and the phase error to be 0.2 deg. The fitted parameters are the tumor absorption $[\mu_a^{(t)}]$ and reduced scattering coefficient $[\mu_s'^{(t)}]$, the tumor diameter (d), and the position of the tumor along the x axis $[x^{(t)}]$ and z axis $[z^{(t)}]$. The x axis is taken along the scanned line whereas the z axis is defined by the line joining the source and detector. We took $z = 0$ to be at half way between the source and the detector (see

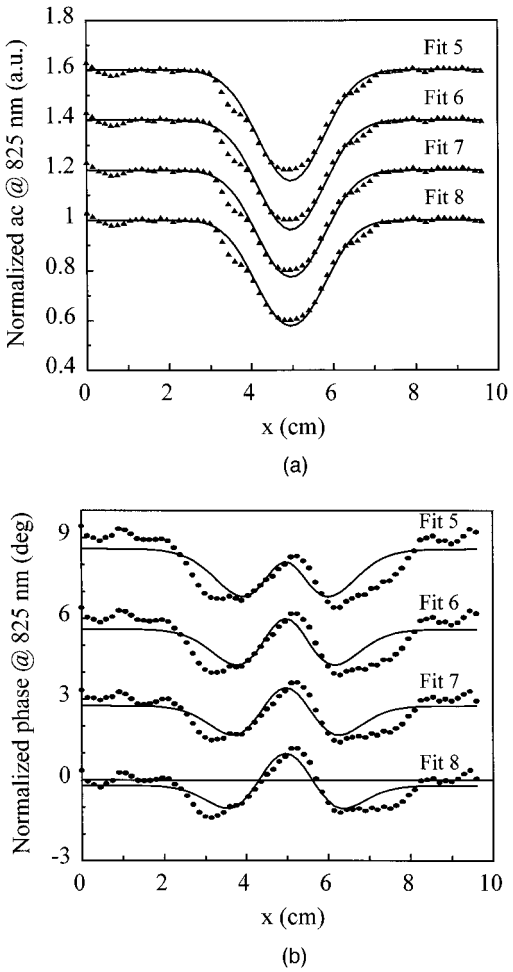

Fig. 6. Normalized data at 825 nm and fits with the analytical solution for the sphere-in-slab problem (curves). (a) ac, solid triangles; (b) phase, solid circles. The four fits [numbered 5–8 in (a) and (b)] correspond to the four different background phase curves shown in Fig. 4(b). In (a), the ac data and fits numbered 5, 6, and 7 were shifted by 0.6, 0.4, and 0.2 a.u., respectively, for clarity. In (b), the phase data and fits numbered 5, 6, and 7 were shifted by 9, 6, and 3 deg, respectively, for clarity.

Fig. 1). Consequently, $z^{(t)}$ gives the depth of the tumor because $L/2 + z^{(t)}$ and $L/2 - z^{(t)}$ are the distances between the tumor and the two compression glass plates (recall that the separation between the plates L is 4 cm in this case). By considering only one projection, i.e., only one particular orientation of the glass plates, we cannot distinguish the positive z side from the negative z side (source and detector are exchangeable for the reciprocity theorem). Therefore, we can measure only the absolute value $|z^{(t)}|$. For the optical coefficients of healthy breast tissue (the background medium), we assumed the literature values shown in Table 1 (Ref. 15). The index of refraction was taken to be 1.4 (Ref. 16), and we assumed no difference between the index of refraction of the tumor $[n^{(t)}]$ and that of healthy tissue (n_0).

Table 2 reports the tumor size, coordinates, and optical coefficients recovered from the eight fits (four at 690 nm and four at 825 nm). Table 2 also shows

Table 1. Assumed Values of the Absorption Coefficient (μ_{a0}), Reduced Scattering Coefficient (μ_{s0}'), and Refractive Index (n_0) of the Background, Healthy Breast Tissue at the Two Wavelengths Considered[a]

Parameter	690 nm	825 nm
μ_{a0} $(\text{cm}^{-1})^b$	0.03	0.04
μ_{s0}' $(\text{cm}^{-1})^b$	12	11
$n_0 = n^{(t)c}$	1.4	1.4

[a]We assume no refractive-index mismatch between healthy and cancerous tissue $[n_0 = n^{(t)}]$.
[b]Ref. 15.
[c]Ref. 16.

the reduced χ^2 ($\chi_\nu^2 = \chi^2/60$) for each fit. These results indicate that this papillary cancer absorbs and scatters near-infrared light more strongly than the surrounding healthy tissue. A higher absorption of malignant tumors *in vivo* has also been reported by Fishkin *et al.*[17] The recovered position and size of the tumor at the two wavelengths agree well. Nevertheless, we observe that the size of the tumor measured at the two wavelengths may be different if oxyhemoglobin and deoxyhemoglobin have different spatial distributions around the tumor. We obtained the overall results for the fitted parameters by performing a weighted average (with $1/\chi_\nu^2$ as the weights) of the results of the different fits. This average assigns a higher weight to the parameters that correspond to the better fits of our model to the data. We estimate the errors in the tumor parameters determined by the ambiguity in the choice of the phase background curve by comparing the recovered parameters in the eight fits. The choice of the background curve is a crucial step in our approach, and to some extent this choice is arbitrary. For this reason, it is relevant to estimate the sensitivity of the recovered parameters to the choice of the background curve. This estimate is given by the errors reported in Table 3. These errors indicate the precision of our method rather than its accuracy. We list the overall results for the tumor size, position, and optical properties in Table 3. The recovered tumor size (2.1 ± 0.2 cm) is comparable with the size measured after surgery (1.6 cm). One should not expect a perfect agreement because of the ambiguity in the size definition and because our method recovers the diameter of an assumed spherical tumor, which is clearly an idealization of the actual tumor (the pathologist reported the tumor size in three dimensions to be $1.6 \times 1.5 \times 0.9$ cm^3). The recovered z coordinate of the tumor is essentially 0, indicating that the tumor should be located half way between the compression plates. However, in the optical mammogram taken on the same breast in the perpendicular view (craniocaudal), the tumor appears to be closer to the detector, i.e., off center. The craniocaudal projection does not allow us to specify exactly the value of $|z^{(t)}|$ because of the geometric effects induced by breast compression, but we can estimate a value of $|z^{(t)}| \sim 0.5$–1.0 cm. This result indicates that our recovery of $|z^{(t)}|$ is correct to within 0.5–1.0 cm. From the

Table 2. Values of the Fitted Parameters for the Eight Fits Performed[a]

Fit	λ (nm)	d (cm)	$x^{(t)}$ (cm)	$\lvert z^{(t)}\rvert$ (cm)	$\mu_a^{(t)}$ (cm^{-1})	$\mu_s'^{(t)}$ (cm^{-1})	χ_ν^2
1	690	1.9	4.87	0.006	0.118	14.1	8.0
2	690	2.1	4.86	0.006	0.093	14.8	6.2
3	690	2.2	4.88	0.006	0.082	15.3	5.2
4	690	2.2	4.86	0.007	0.070	15.2	2.8
5	825	1.8	4.97	0.008	0.127	11.9	8.0
6	825	1.9	4.97	0.008	0.096	12.7	7.1
7	825	2.1	4.97	0.010	0.077	12.8	4.1
8	825	2.2	4.96	0.007	0.068	13.0	3.5

[a]The resulting curves of the simultaneous ac and phase fits are shown in Figs. 5 and 6.

absorption coefficients at the two wavelengths, we calculated the hemoglobin concentration and saturation in the tumor area,[18] under the assumption that the absorption of light in the tumor [$\mu_a^{(t)}$] is due solely to hemoglobin. We comment on this assumption in Section 5. The results for oxyhemoglobin concentration $[HbO_2]^{(t)}$, deoxyhemoglobin concentration $[Hb]^{(t)}$, total hemoglobin concentration $[Hb]_{tot}^{(t)} = [HbO_2]^{(t)} + [Hb]^{(t)}$, and hemoglobin saturation $Y^{(t)} = [HbO_2]^{(t)}/[Hb]_{tot}^{(t)}$ in the tumor area are also reported in Table 3. We obtained the errors in the hemoglobin-related parameters by propagating the errors in the absorption coefficients through the expressions for $[Hb]^{(t)}$, $[HbO_2]^{(t)}$, and $Y^{(t)}$ (Ref. 19).

5. Discussion

The first two steps on which our approach is based [(1) finding $ac_{bgr}(x)$ and $\Phi_{bgr}(x)$ by fitting the data points out of the tumor area with a smooth curve, and (2) divide the measured ac by $ac_{bgr}(x)$ and subtract $\Phi_{bgr}(x)$ from the measured phase] are required by the relevance of the edge effects in our raw data. In the absence of edge effects, these two steps would not be needed, and in the presence of weaker edge effects they would be less critical. In the presence of strong edge effects, our method can not be applied if the tumor is close to the edge of the image. An effective way to suppress the edge effects in the raw data, thus allowing the general applicability of our method, would be embedding the breast in a strongly scattering substance that matches the breast optical properties. This approach has already been proposed and tested,[20–24] and it has the advantage that it would not require a redesign of the LIMA.

Table 3. Size, Position, Optical Coefficients, Hemoglobin Concentration, and Hemoglobin Saturation of the Breast Tumor (a papillary cancer) Obtained *in vivo* with our Noninvasive Optical Method

Parameter	Value	Units
d	2.1 ± 0.2	cm
$x^{(t)}$	4.91 ± 0.05	cm
$\lvert z^{(t)}\rvert$	0.007 ± 0.002	cm
$\mu_a^{(t)}$ (690 nm)	0.084 ± 0.014	cm^{-1}
$\mu_a^{(t)}$ (825 nm)	0.085 ± 0.017	cm^{-1}
$\mu_s'^{(t)}$ (690 nm)	15.0 ± 0.3	cm^{-1}
$\mu_s'^{(t)}$ (825 nm)	12.7 ± 0.3	cm^{-1}
$[HbO_2]^{(t)}$	28 ± 9	μM
$[Hb]^{(t)}$	12 ± 4	μM
$[HbO_2]^{(t)} + [Hb]^{(t)}$	40 ± 10	μM
$Y^{(t)} = [HbO_2]^{(t)}/([HbO_2]^{(t)} + [Hb]^{(t)})$	71 ± 9	%

The third step of our method consists of fitting the data with the analytical solution for a spherical object in an infinite slab. Of course, the sphere-in-slab model is an abstraction of the real case. Although the infinite slab geometry provides a reasonable model for the compressed breast, the assumed spherical shape of the tumor can be considered only as a first approximation. Also, by sectioning the breast tissue in two parts, the healthy uniform background and the spherical lesion, we oversimplify the complexity of the actual spatial distribution of the optical properties in the breast. Consequently, our approach cannot be seen as a solution to the inverse problem, which would instead provide a three-dimensional distribution of the breast optical properties. Using our simplified model, we are also not able to describe the internal morphology of the lesion. A strong assumption made in the fit is the homogeneity of the healthy tissue. This is not the case, and the tissue inhomogeneity has visible effects on the measured data. Nevertheless, the fits shown in Figs. 5 and 6 correctly reproduce the main features of the ac and phase traces, and the data fluctuations that are due to the tissue inhomogeneity can be seen as a superimposed nonrandom noise.

Despite the above-mentioned limitations, we believe that our frequency-domain method provides some progress in the field of optical mammography because it demonstrates the feasibility of the noninvasive optical characterization of breast tumors *in vivo*. The *N*-parameter-based optical mammograms shown in Fig. 2 successfully detect the breast tumor, but they are incapable of giving information about its optical properties. With the additional analysis presented in this paper, we can determine the size, the position, the optical properties, and the hemoglobin concentration and saturation of the detected tumor. Recent studies have shown that the optical characterization can be achieved only for spheres having a diameter larger than approximately 1 cm (Refs. 25, 26). Even for smaller tumors, however, our method will still be capable of discerning absorbing from scattering lesions and to quantify the hemoglobin satu-

ration. In fact, for tumors with $d < 1$ cm, it is still possible to determine the products $\mu_a^{(t)}d^3$ and $\mu_s'^{(t)}d^3$. Because the hemoglobin saturation $[Y^{(t)}]$ depends only on the ratio $\mu_a^{(t)}(\lambda_1)/\mu_a^{(t)}(\lambda_2)$ (where λ_1 and λ_2 are the two wavelengths employed), the common factor d^3 cancels in the expression for $Y^{(t)}$, so that the hemoglobin saturation can be quantified.

In this preliminary application, we used values reported in the literature for the background optical properties μ_{a0} and μ_{s0}'. We observe that this can be avoided, thus making our approach self-contained, by measuring the average optical properties of the breast in a position far from the tumor. Several methods have been employed successfully to quantify the average optical properties of tissues.[11,17,19,27] The sensitivity of the recovered tumor optical properties on the assumed values for the background optical coefficients is an important issue. To investigate this issue, we repeated the fit to the data at 690 nm [phase background 4 in Fig. 3(b)] for different combinations of μ_{a0} and μ_{s0}' within the range of *in vivo* values reported in the literature[15,28] [$0.02\ \text{cm}^{-1} \le \mu_{a0}$ (690 nm) $\le 0.04\ \text{cm}^{-1}$; $8\ \text{cm}^{-1} \le \mu_{s0}'$ (690 nm) $\le 10\ \text{cm}^{-1}$]. In this range of values of μ_{a0} and μ_{s0}', we found that the dependence of the recovered tumor optical coefficients $[\mu_a^{(t)}, \mu_s'^{(t)}]$ on the assumed background coefficients (μ_{a0}, μ_{s0}') is approximately described by the following relationships: $\mu_a^{(t)} \approx 2\,\mu_{a0} - 0.005\,\mu_{s0}' + 0.07\ \text{cm}^{-1}$; $\mu_s'^{(t)} \approx \mu_{s0}' + 3\ \text{cm}^{-1}$. The tumor always results in more absorbing and more scattering than the background tissue. If we denote the errors in μ_{a0} and μ_{s0}' by $\Delta\mu_{a0}$ and $\Delta\mu_{s0}'$, respectively, we can see that the corresponding errors in $\mu_a^{(t)}$ $[\Delta\mu_a^{(t)}]$ and $\mu_s'^{(t)}$ $[\Delta\mu_s'^{(t)}]$ are given by $\Delta\mu_a^{(t)} \approx 2\,\Delta\mu_{a0} + 0.005\,\Delta\mu_{s0}'$, and $\Delta\mu_s'^{(t)} \approx \Delta\mu_{s0}'$. These errors in $\mu_a^{(t)}$ and $\mu_s'^{(t)}$ must be added to the errors reported in Table 3, which take into account only the uncertainty in the choice of the background phase curve. For example, a 10% error in the background optical coefficients would contribute an error of approximately $0.01\ \text{cm}^{-1}$ in $\mu_a^{(t)}$ and approximately $1\ \text{cm}^{-1}$ in $\mu_s'^{(t)}$.

To calculate the hemoglobin concentration and saturation in the tumor area, we assumed that hemoglobin is the only absorber in breast tissue, although it is known that water and lipids also have near-infrared absorption bands.[29] Because our current prototype for frequency-domain optical mammography collects data at only two wavelengths, we made this assumption. A more accurate determination of the hemoglobin concentration would require the quantification of the water content, which can be obtained by employing more than two wavelengths[30] or a full spectrum.[15,29] However, we note that, because reported water concentrations in the breast are of the order of 20 M and can be as low as 5 M (Refs. 29, 30), the water absorption at our wavelengths gives a relatively small contribution ($\lesssim 0.002\ \text{cm}^{-1}$ at 690 nm, $\lesssim 0.010\ \text{cm}^{-1}$ at 825 nm) that falls within our experimental error in $\mu_a^{(t)}$.

6. Conclusion

We have presented a method for the noninvasive sizing and optical characterization of breast tumors *in vivo*. This method is based on diffusion theory and on frequency-domain spectroscopy in the near infrared. In the case reported here, we found that the breast tumor (a papillary cancer) is more absorbing and more scattering than the healthy tissue. Its total hemoglobin concentration $[\text{Hb}]_{\text{tot}}^{(t)}$ is $40 \pm 10\ \mu\text{M}$, whereas its hemoglobin saturation is $71 \pm 9\%$. These results provide the clinical examiner with several parameters that characterize the tumor, namely the size, the absorption coefficient, the reduced scattering coefficient, the hemoglobin concentration, and the hemoglobin saturation. This information complements the detectability of breast lesions afforded by frequency-domain optical mammography, and it is expected to enhance the specificity of frequency-domain optical mammography.

We thank Enrico Gratton for useful discussions and W. Haensch for providing the pathology data. This research is supported by NIH grant CA57032 and by Whitaker—NIH grant RR10966. K. T. Moesta and P. M. Schlag acknowledge support from the Schott-Zeiss Scientific Foundation.

References and Notes

1. M. Cutler, "Transillumination of the breast," Surg. Gynecol. Obstet. **48,** 721–727 (1929).
2. C. M. Gros, Y. Quenneville, and Y. Hummel, "Diaphanologie mammaire," J. Radiol. Electrol. Med. Nucl. **53,** 297–306 (1972).
3. E. Carlsen, "Transillumination light scanning," Diagn. Imaging **4,** 28–34 (1982).
4. A. Alveryd, I. Andersson, K. Aspegren, G. Balldin, N. Bjurstam, G. Edström, G. Fagerberg, U. Glas, O. Jarlman, S. A. Larsson, E. Lidbrink, H. Lingaas, M. Löfgren, C.-M. Rudenstam, L. Strender, L. Samuelsson, L. Tabàr, A. Taube, H. Wallberg, P. Åkesson, and D. Hallberg, "Lightscanning versus mammography for the detection of breast cancer in screening and clinical practice," Cancer **65,** 1671–1677 (1990).
5. Y. Yamashita and M. Kaneko, "Visible and infrared diaphanoscopy for medical diagnosis," in *Medical Optical Tomography: Functional Imaging and Monitoring*, G. J. Müller, B. Chance, R. R. Alfano, S. R. Arridge, J. Beuthan, E. Gratton, M. Kaschke, B. R. Masters, S. Svanberg, and P. van der Zee, eds., Vol. IS11 of SPIE Institute Series (SPIE Press, Bellingham, Wash., 1993), pp. 283–316.
6. M. A. Franceschini, K. T. Moesta, S. Fantini, G. Gaida, E. Gratton, H. Jess, W. W. Mantulin, M. Seeber, P. M. Schlag, and M. Kaschke, "Frequency-domain techniques enhance optical mammography: initial clinical results," Proc. Natl. Acad. Sci. USA **94,** 6468–6473 (1997).
7. H. Jess, H. Erdl, K. T. Moesta, S. Fantini, M. A. Franceschini, E. Gratton, and M. Kaschke, "Intensity-modulated breast imaging: technology and clinical pilot study results," in *Advances in Optical Imaging and Photon Migration*, R. R. Alfano and J. G. Fujimoto, eds., Vol. 2 of OSA Trends in Optics and Photonics (Optical Society of America, Washington, D.C., 1996), pp. 126–129.
8. K. T. Moesta, S. Fantini, H. Jess, S. Totkas, M. A. Franceschini, M. Kaschke, and P. M. Schlag, "Contrast features of breast cancer in frequency-domain laser scanning mammography," J. Biomed. Opt. **3**(2) (1998).
9. S. Fantini, M. A. Franceschini, G. Gaida, E. Gratton, H. Jess,

W. W. Mantulin, K. T. Moesta, P. M. Schlag, and M. Kaschke, "Frequency-domain optical mammography: edge effect corrections," Med. Phys. **23,** 149–157 (1996).
10. D. A. Boas, M. A. O'Leary, B. Chance, and A. G. Yodh, "Scattering of diffuse photon density waves by spherical inhomogeneities within turbid media: analytic solution and applications," Proc. Natl. Acad. Sci. USA **91,** 4887–4891 (1994).
11. M. S. Patterson, B. Chance, and B. C. Wilson, "Time resolved reflectance and transmittance for the non-invasive measurement of optical properties," Appl. Opt. **28,** 2331–2336 (1989).
12. R. C. Haskell, L. O. Svaasand, T. T. Tsay, T. C. Feng, M. S. McAdams, and B. J. Tromberg, "Boundary conditions for the diffusion equation in radiative transfer," J. Opt. Soc. Am. A **11,** 2727–2741 (1994).
13. The Photon Migration Imaging code is available on the World Wide Web at http://dpdw.eotc.tufts.edu/boas/PMI/pmi.html. The developers of the code are D. Boas, X. Li, M. O'Leary, B. Chance, A. Yodh, M. Ostermeyer, S. Jacques, G. Nishimura, and S. Walker.
14. B. A. Feddersen, D. W. Piston, and E. Gratton, "Digital parallel acquisition in frequency domain fluorometry," Rev. Sci. Instrum. **60,** 2929–2936 (1989).
15. H. Heusmann, J. Kölzer, and G. Mitic, "Characterization of female breasts *in vivo* by time resolved and spectroscopic measurements in near infrared spectroscopy," J. Biomed. Opt. **1,** 425–434 (1996).
16. F. P. Bolin, L. E. Preuss, R. C. Taylor, and R. J. Ference, "Refractive index of some mammalian tissues using a fiber optic cladding method," Appl. Opt. **28,** 2297–2302 (1989).
17. J. B. Fishkin, O. Coquoz, E. R. Anderson, M. Brenner, and B. J. Tromberg, "Frequency-domain photon migration measurements of normal and malignant tissue optical properties in a human subject," Appl. Opt. **36,** 10–20 (1997).
18. E. M. Sevick, B. Chance, J. Leigh, S. Nioka, and M. Maris, "Quantitation of time- and frequency-resolved optical spectra for the determination of tissue oxigenation," Anal. Biochem. **195,** 330–351 (1991).
19. S. Fantini, M. A. Franceschini, J. S. Maier, S. A. Walker, B. Barbieri, and E. Gratton, "Frequency-domain multichannel optical detector for non-invasive tissue spectroscopy and oximetry," Opt. Eng. **34,** 32–42 (1995).
20. W. W. Mantulin, S. Fantini, M. A. Franceschini, S. A. Walker, J. S. Maier, and E. Gratton, "Tissue optical parameter map generated with frequency-domain spectroscopy," in *Biomedical Optoelectronic Instrumentation*, J. A. Harrington, D. M. Harris, and A. Katzir, eds., Proc. SPIE **2396,** 323–330 (1995).
21. S. Zhou, C. Xie, S. Nioka, H. Liu, Y. Zhang, and B. Chance, "Phased array instrumentation appropriate to high precision detection and localization of breast tumor," in *Optical Tomography and Spectroscopy of Tissue: Theory, Instrumentation, Model, and Human Studies II*, B. Chance and R. R. Alfano, eds., Proc. SPIE **2979,** 98–106 (1997).
22. A. Yodh, "The American experience in optical mammography," presented at the conference on Breast Cancer Detection by Near Infrared Spectroscopy and Imaging, Berlin, Germany, 6–7 June 1997.
23. J. H. Hoogenraad, M. B. van der Mark, S. B. Colak, G. W.'t Hooft, and E. S. van der Linden, "First results from the Philips optical mammoscope," in *Photon Propagation in Tissues III*, D. Benaron, B. Chance, and M. Ferrari, eds., Proc. SPIE **3194,** 184–190 (1998).
24. X. Wu, L. Stinger, and G. Faris, "Determination of tissue properties by immersion in a matched scattering fluid," in *Optical Tomography and Spectroscopy of Tissue: Theory, Instrumentation, Model, and Human Studies II*, B. Chance and R. R. Alfano, eds., Proc. SPIE **2979,** 300–306 (1997).
25. D. A. Boas, M. A. O'Leary, B. Chance, and A. G. Yodh, "Detection and characterization of optical inhomogeneities with diffuse photon density waves: a signal-to-noise analysis," Appl. Opt. **36,** 75–92 (1997).
26. G. Ledanois and J. Virmont, "Optical medical diagnostic and imaging," in *Photon Propagation in Tissues III*, D. Benaron, B. Chance, and M. Ferrari, eds., Proc. SPIE **3194,** 405–408 (1998).
27. T. J. Farrel, M. S. Patterson, and B. Wilson, "A diffusion theory model of spatially resolved, steady-state diffuse reflectance for the noninvasive determination of tissue optical properties *in vivo*," Med. Phys. **19,** 879–888 (1992).
28. K. A. Kang, B. Chance, S. Zhao, S. Srinivasan, E. Patterson, and R. Troupin, "Breast tumor characterization using near-infra-red spectroscopy," in *Photon Migration and Imaging in Random Media and Tissues*, B. Chance and R. R. Alfano, eds., Proc. SPIE **1888,** 487–499 (1993).
29. V. Quaresima, S. J. Matcher, and M. Ferrari, "Identification and quantification of intrinsic optical contrast for near-infrared mammography," Photochem. Photobiol. **67,** 4–14 (1998).
30. B. J. Tromberg, O. Coquoz, J. B. Fishkin, T. Pham, E. R. Anderson, J. Butler, M. Cahn, J. D. Gross, V. Venugopalan, and D. Pham, "Non-invasive measurements of breast tissue optical properties using frequency-domain photon migration," Philos. Trans. R. Soc. London Ser. B **352,** 661–668 (1997).